Letters in Applied NanoBioScience
Open-Access Journal (ISSN: 2284-6808)

Article
Volume 12, Issue 2, 2023, 48
https://doi.org/10.33263/LIANBS122.048

Development of High Coercivity/High Fluorescence Hybrid nanostructures

Dipti Rawat [1,*], Ragini Raj Singh [1]

[1] Nanotechnology Laboratory, Department of Physics and Materials Science, Jaypee University of Information Technology, Waknaghat, Solan 173234, H.P., India
* Correspondence: ashadiptirawat@gmail.com (D.P.);

Scopus Author ID 57203592140

Received: 13.01.2022; Accepted: 15.02.2022; Published: 19.03.2022

Abstract: The study concentrated on the prospects of multifunctional core-shell that can incorporate multiple functions simultaneously. For the sharp and precise assembling of core-shell nanostructures (CS-Ns) combining ferromagnetic-core and semiconducting-shell into a single material with mouldable fluorescence and magnetic features, the seed-mediated aqueous growth technique was flourished. $SrFe_{12}O_{19}$/CdS CS-Ns were designed to gratify the requirement of magneto-fluorescent features in a solo unit. Characterization techniques such as XRD, VSM and photoluminescence spectroscopy (PL) was used to analyze the as-synthesized CS-Ns. XRD spectra confirm the CS-Ns formation with the pure phase. PL results show that the CS-Ns follow the emission profile of the CdS shell. CS-Ns formation leads to a much better particle size distribution. In VSM analysis, it was observed that the saturation of the hysteresis loop is decayed many times as that of the bare core because of the semiconducting shell covering over the core. Altogether the results were in good agreement with one another. Because of the permanent magnetic nature of $SrFe_{12}O_{19}$ (1000°C), these CS-Ns are used in the magnetic separation process, where the ferromagnetic core aids in magnetic manipulation, and the fluorescent shell aids in detecting the path of the separated entity.

Keywords: core-shell nanostructures; ferromagnetic; semiconducting; magneto-fluorescent; magnetic seperation.

1. Introduction

The manufacturing of CS-Ns, which are made up of an inner core substance coated by a shell made of a separate material, has recently gotten a lot of attention [1-10]. The fact that core-shell nanoparticles can display increased physical and/or chemical properties has drawn a lot of attention. Furthermore, by modifying, for example, their size, shell thickness, and architectures, core-shell particles with distinctly different properties compared to those of the constituent materials can be developed [11-15]. Several research initiatives are underway to synthesize highly efficient core-shell materials for use in various domains, including optoelectronic devices, biomedical imaging, catalysis, and plasmonic [16-20].

This study used the seed-mediated growth method to synthesize core-shell nanostructures via aqueous solvent mean. $SrFe_{12}O_{19}$/CdS core-shell hybrid nanostructures were synthesized for the magneto-fluorescent core-shell design. Initially, the magnetic $SrFe_{12}O_{19}$ nanoparticles were produced using the Sol-gel method and then coated with CdS QDs. The inner core that is $SrFe_{12}O_{19}$ provides the magnetic results and the CdS quantum dots shell provides the fluorescent results. Owing to the permanent magnetic characteristic of $SrFe_{12}O_{19}$

and the excellent fluorescence nature of CdS QDs, these hybrid core-shell nanostructures can find application in magnetic cell separation where the magnetic core help to drag the nanoparticle fluorescent shell helps in cells path tracking [21].

2. Materials and Methods

For the $SrFe_{12}O_{19}$ synthesis, metal, nitrates, and citric acid was used. For the CdS QDs synthesis, Cadmium chloride, Ammonium chloride, thiourea, and 2-mercaptoethenol (capping agent) were used. Ammonia solution was used for maintaining the right pH. A two-step synthesis process was used to derive $SrFe_{12}O_{19}$/CdS CSNs. Firstly, $SrFe_{12}O_{19}$ ferrite nanoparticles were synthesized distinctly, and then these ferrite nanoparticles were dispersed in the solution of CdS to form the CS-Ns. Seed-mediate-growth-approach, combining sol-gel and solution growth methods, was efficaciously processed to fabricate magneto-fluorescent core-shell hybrid nanostructures of $SrFe_{12}O_{19}$/CdS via an aqueous pathway, leading to improved magneto-fluorescent properties. A brief idea for the synthesis of QDs, ferrites, and CSNs was described in detail in papers [2, 21]. Magnetic nanoparticles (MNP) were prepared separately in the first stage, and then in the second stage, MNP was dissolved in CdS solution to form CS-Ns. MNPs synthesis is achieved by opting for water as solvent. Metal nitrates were dissolved in water, followed by mixing citric acid solution in the nitrate solution, after optimizing the reaction conditions, a 1:3 molar ratio of nitrates: citric acid was taken. pH was continued at 8.5. Afterward, the solution temperature was kept to be 80°C till sol was changed to gel. Prepared gel was then desiccated in the oven at 110°C for 24 h; the dried powder was then heated in a furnace at 1000°C temperature range. In the second step, cadmium precursor was added in 50 mL of distilled water, then heated and stirred continuously until the temperature reached 70^{o}C and the pH was maintained at 8.5. MNP (loading of 0.1 g) was then added to the solution, followed by thiourea and mercaptoethanol. Between the CdS shell creation and the synthesis of CS-Ns, a certain quantity of MPs, which are core materials, is introduced. MPs 0.1 g denotes the precise amount of 0.1 g of MPs that were used to make MPs (0.1) CdS CS-Ns. The solution was then heated for 3 hours at 70°C with constant stirring.

3. Results and Discussion

This section deals with the various results we evaluated from the as-synthesized core, shell, and CS-Ns.

3.1. XRD analysis.

XRD spectra for the bare $SrFe_{12}O_{19}$, bare CdS, and the $SrFe_{12}O_{19}$/CdS CSNs are shown in Figure 1. Graph (a) illustrates the XRD spectra for the CdS QDs where the peaks indexed at (111), (220), and (311) indicate the cubic structure for CdS QDs (JCPDS80-0019). Pattern (b) shows the XRD spectra of $SrFe_{12}O_{19}$ annealed at 1000^{o}C with the peaks indexed at (105), (110), (008), (107), (114), (201), (205), (304), and (220) indicate the hexagonal structure (JCPDS 84-1531). Pattern (c) illustrates the spectra for $SrFe_{12}O_{19}$/CdS CS-Ns with 0.1 g core loading.

$SrFe_{12}O_{19}$ and CdS QDs peaks in CS-Ns are at identical positions as their respective spectra. Additionally, in the case of CdS QDs coated $SrFe_{12}O_{19}$/CdS CSNs, the comparative intensity of the peaks reflecting the magnetite phase gets reduced. The lesser intensity of hexaferrite peak could indicate more CdS QDs covering core ferrite [21]. The spectra's nature supports the creation of CS-Ns. Calculate crystallite sizes of the $SrFe_{12}O_{19}$ and CdS QDs is

23.9 nm and 1.6 nm, respectively. Calculation of crystallite size for CS-Ns using XRD is impossible as identical peaks for the core and shell are found in the CS-Ns spectra [22].

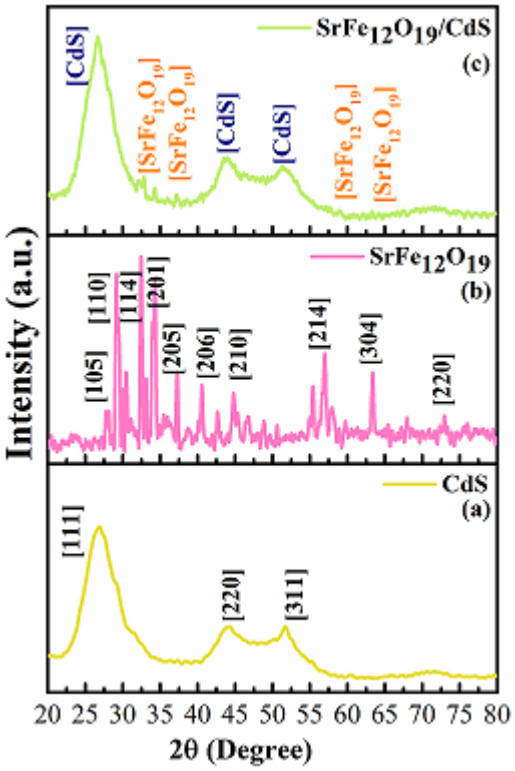

Figure 1. Shows the XRD spectra for: (**a**) CdS; (**b**) $SrFe_{12}O_{19}$; **(c)** $SrFe_{12}O_{19}$/CdS CSNs.

From the XRD results, it was confirmed that the CSNs formation is successfully achieved because if CSNs is not prepared successfully, there might be chances of alloy formation, which result in the shift in the peak position of the core as well as a shell, or there may be chances of non appropriate covering of core with the shell. But decaying in magnetic peak intensity with the CSNs formation validates that the core is perfectly covered with the shell.

3.2. Photoluminescence (PL) analysis.

PL spectra were recorded at ambient temperature at a static wavelength of 350 nm. Figure 2. shows the emission profile for CdS, $SrFe_{12}O_{19}$, and the CS-Ns of $SrFe_{12}O_{19}$/CdS. For CdS QDs, luminescence is achieved at 489.05 nm, 464.21 nm, and 533.23 nm; due to the varied distribution of particle size of QDs. $SrFe_{12}O_{19}$ core depicts no luminescence other than the water's Raman peak at 402 nm, which is confirmed by taking the $SrFe_{12}O_{19}$ spectra at changed excitation wavelengths where a continuous shift in peak position has been detected with each scan. CS-Ns follow the same emission profile as that of CdS, except that the peak positioned at 464 disappeared with the CS-Ns formation. We can say that better distribution of particle size is attended with the CS-Ns creation. The graph also confirmed that the luminescence in the CS-Ns system is merely due to the shell CdS only. Core has insignificant partaking in luminescences of magneto-fluorescent CS-Ns; there is no mixing or any complex creation during the CSNs creation.

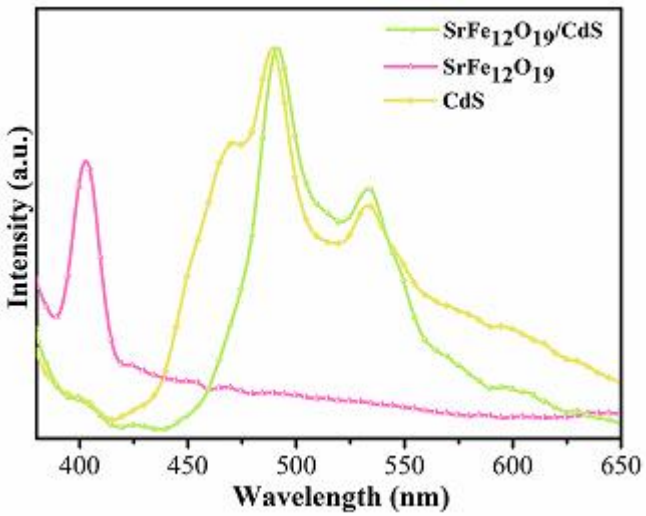

Figure 2. PL spectra for: CdS, $SrFe_{12}O_{19}$; and $SrFe_{12}O_{19}$/CdS CSNs.

$SrFe_{12}O_{19}$/CdS spectra show the slight shift in peak positions as that of bare CdS due to the substrate effect of $SrFe_{12}O_{19}$ core on the CdS seeds. CSNs formed with core annealed at 1000ºC show no extra peak other than that of CdS as was observed with same CSNs formed with core annealed at 700°C [2]. CSNs formed with 1000°C annealed core are highly intact and show the luminescence only as that of CdS profile with no additional emission peak. Table 1 shows the peak positions and intensities of $SrFe_{12}O_{19}$, CdS QDs, and $SrFe_{12}O_{19}$/CdS CSNs.

Table 1. The intensity and respective peak positions of $SrFe_{12}O_{19}$, CdS QDs, and $SrFe_{12}O_{19}$/CdS CS-Ns.

S. No	Sample name	Peak Positions				Peak Intensity			
		P_1	P_2	P_3	P_4	I_1	I_2	I_3	I_4
1.	$SrFe_{12}O_{19}$	402	-	-	-	100	-	-	-
2.	CdS	-	464	489	533	-	105	136	85
3.	$SrFe_{12}O_{19}$/CdS	-	-	490	533	-	-	136	91

3.3. Magnetic analysis.

Figure 3. (a and b) shows the M-H loop for the $SrFe_{12}O_{19}$ and $SrFe_{12}O_{19}$/CdS CSNs. M-H curves are taken in the range of -10 to +10 KOe at ambient temperature. Since the shell material that is CdS is completely diamagnetic, we have shown the M-H curve for the core and CS-Ns only. From graph (a), it is clearly seen that the saturation magnetization (M_s) is near about 27 emu/g, which on switching to the CSNs is declined to many times and remain nearly about 1.5 emu/g. This drastic decay in M_s value with the creation of CS-Ns is owed because of the development of magnetically departed CdS seeds over $SrFe_{12}O_{19}$. With the creation of CS-Ns, factors such as anisotropy constant (K), retentivity (M_r), squareness ratio, switching field distribution (SFD), etc., have been affected, which were discussed later, and the parameters were inscribed in Table 2.

The noteworthy extreme evidence in the process of CS-Ns creation is the denial of anisotropy (K). K value is calculated using the formula, $K= (H_c \times M_s)/2$. The deficit directs toward the intactness of the CS-Ns system; meanwhile, if the CS-Ns system is not undamaged, the risk of intermixing of core and shell entity at the interface might be possible, impacting K value. Strong coupling is shown by good squareness and higher remanence.

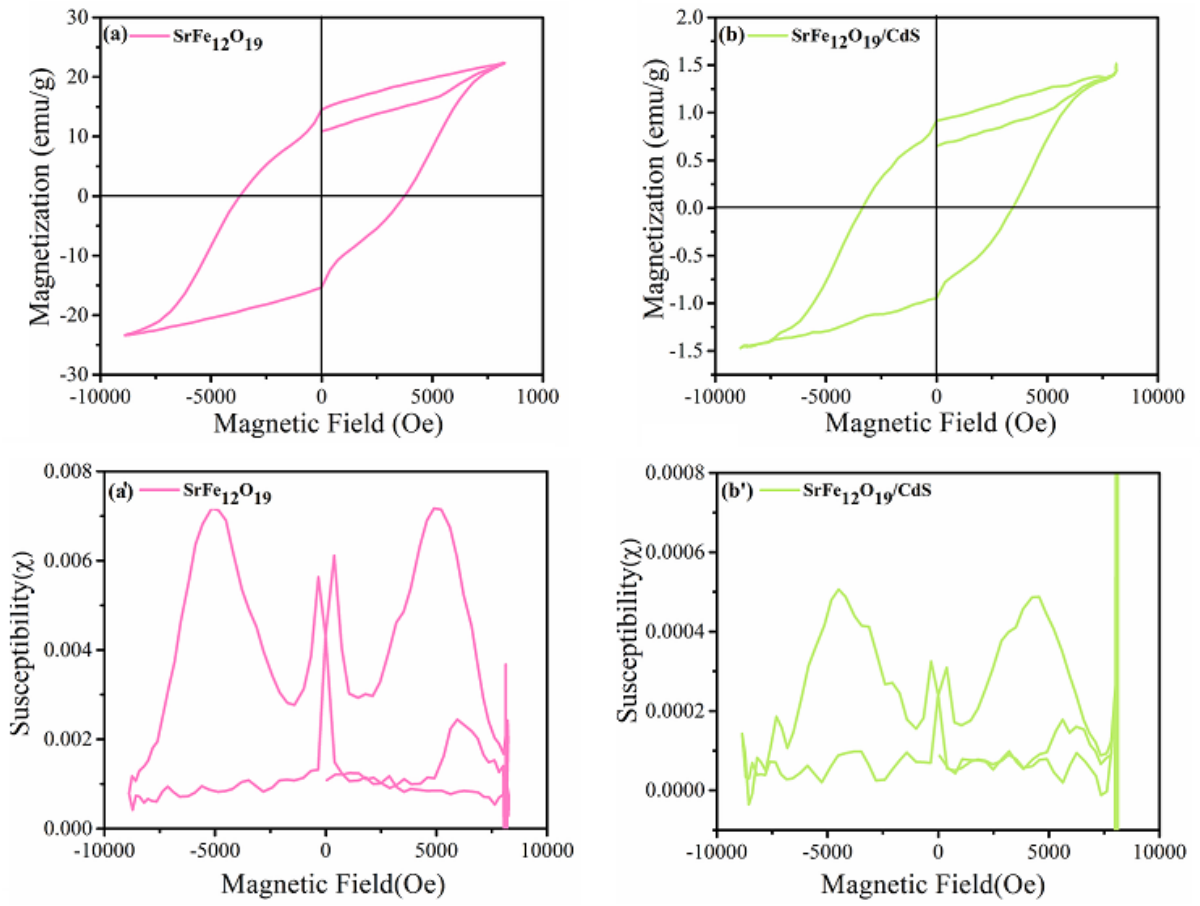

Figure 3. Shows the Hysteresis curve for: **(a)** $SrFe_{12}O_{19}$; **(b)** $SrFe_{12}O_{19}$/CdS CSNs; and the diffrential susceptibility cuve for: **(a')** $SrFe_{12}O_{19}$; **(b')** $SrFe_{12}O_{19}$/CdS CSNs.

Table 2. Magnetic parameters for $SrFe_{12}O_{19}$ and $SrFe_{12}O_{19}$/CdS CSNs.

S. No	Sample name	Coercivity (Hc) Oe	Retentivity (Mr) emu/g	Saturation (M_S) emu/g	Anisotropy (K) erg/cm^3	μ_b	SFD
1.	$SrFe_{12}O_{19}$	3681	14	22	40500	4.18	2
2.	$SrFe_{12}O_{19}$/CdS	3475	1	1.4	2360	0.3	1

The 1st order differential susceptibility curve for the core and CS-Ns are shown in Figure 3. (a' and b'). Derivative spectroscopy was used to compute the SFD. The information on spin orientation at high and low magnetic fields is provided by SFD. This information is critical for comparing CSNs to bare core and shell structures. When switching from bare $SrFe_{12}O_{19}$ to CS-Ns, a significant difference in SFD was observed. The SFD was derived using the formula SFD = $\Delta H/H_C$, where ΔH is the FWHM of the simple M-H loop differentiated curve [23].

The first peak on the samples' differential curve is a broad hump from which we calculated the FWHM for calculating the system's SFD, and this broad hump also points to the hardness of magnetic material, and this broad hump is a significant point to distinguish between hard and soft ferrites [23-24]. 2nd peak in the differential curve of all the samples is due to a steeper slope in the weak magnetic field area. As we proceed from bare ferrite to CS-Ns, the peak's intensity decreases in the same way as the slope decreases. It is obvious from the values that the SFD value of pure ferrite in bulk is higher than the combined system of CS-Ns, indicating that the CS-Ns system has better particle size distribution than bare $SrFe_{12}O_{19}$. In conclusion, the magnetic and optical results can be inferred to validate one another.

4. Conclusions

The synthesis of CS-Ns with magneto-optical properties in a singular entity has been successfully performed. The CdS shell has a well-defined cubical phase, while SrFe12O19 has a hexagonal phase according to structural specifications. The particle size distribution is enhanced with a slight red shift in CS-Ns compared to that of CdS QDs. From magnetic results, it is inveterate that CdS is impeccably grown over the $SrFe_{12}O_{19.}$ Based on optical, magnetic, and structural properties, these nanostructures found applications in various fields, including spintronics and biological cell sorting applications that require a permanent magnetic field.

Funding

This research received no external funding.

Acknowledgments

I extend my sincere thanks to SAIF Panjab University Chandigarh for helping in recording XRD and IIT Roorkee for recording VSM results.

Conflicts of Interest

The authors declare no conflict of interest.

References

1. Rawat, D.; Barman, P.B.; Singh, R.S. Corroboration and efficacy of magneto-fluorescent (NiZnFe/CdS) nanostructures prepared using differently processed core. *Sci. Rep*. **2019**, *9*, 15138, https://doi.org/10.1038/s41598-019-51631-w.
2. Rawat, D.; Sethi, J.; Sahani, S.; Barman, P.B.; Singh, R.S. Pioneering and proficient magneto fluorescent nanostructures: hard ferrite based hybrid structures. *Mater. Sci. Eng. B.* **2021,** *265*, 115017, https://doi.org/10.1016/j.mseb.2020.115017.
3. Kurian, M.; Thankachan, S. Structural diversity and applications of spinel ferrite core-Shell nanostructures-a review. *Open Ceramics* **2021**, *8*, 100179, https://doi.org/10.1016/j.oceram.2021.100179.
4. Shah, K.W.; Huseien, G.F.; Kua, H.W. A State-of-the-Art Review on Core–Shell Pigments Nanostructure Preparation and Test Methods. *Micro*. **2021,** *1*, 55-85, https://doi.org/10.3390/micro1010006.
5. Huang, J.; Long Y.; Songbin, L.; Nan, S.; Qinyuan, Z.; Bo, Z. Dynamic Control of Orthogonal Upconversion in Migratory Core–Shell Nanostructure toward Information Security. *Adv. Funct. Mater.* **2021,** *31*, 2009796, https://doi.org/10.1002/adfm.202170096.
6. Alterary, S.S.; Anfal A. Synthesis, surface modification, and characterization of Fe_3O_4@ SiO_2 core@ shell nanostructure. *Green Process. Synth.* **2021**, *10*, 384-391, https://doi.org/10.1515/gps-2021-0031.
7. Zhang, Y.Z.; Radjenovic, P.M.; Zhou, X.-S.; Zhang, H.; Yao, J.-L.; Li, J.-F. Plasmonic Core–Shell Nanomaterials and their Applications in Spectroscopies. *Adv. Mater.* **2021**, 2005900, https://doi.org/10.1002/adma.202005900.
8. Snellman, M.; Eom, N.; Ek, M.; Messing, M.E.; Deppert, K. Continuous gas-phase synthesis of core–shell nanoparticles via surface segregation. *Nanoscale Adv.* **2021**, *3*, 3041-3052, https://doi.org/10.1039/D0NA01061H.
9. Imran, M. I.; Zouli, N.; Ahamad, T.; Alsheri, S.M.; Chandan, M.R.; Hussain, S.; Aziz, A.; Dar, M.A.; Khan, A. Carbon-coated Fe_3O_4 core–shell super-paramagnetic nanoparticle-based ferrofluid for heat transfer applications. *Nanoscale Adv.* **2021,** *3*, 1962-1975, http://doi.org/10.1039/d1na00061f.
10. Singh, R.; Bhateria, R. Core–shell nanostructures: A simplest two-component system with enhanced properties and multiple applications. *Environ. Geochem. Health* **2021,** *43*, 2459-2482, https://doi.org/10.1007/s10653-020-00766-1.

11. Hara, S.; Aisu, J.; Kato, M.; Aono, T.; Sugawa, K.; Takase, K.; Otsuki, J.; Shimizu, S.; Ikake, H. One-pot synthesis of monodisperse $CoFe_2O_4$@Ag core-shell nanoparticles and their characterization. *Nanoscale Res. Lett.* **2018**, *13*, 1-7, https://doi.org/10.1186/s11671-018-2544-z.
12. Kumar, S.K.; Kumar, V.B.; Paik, P. Recent advancement in functional core-shell nanoparticles of polymers: synthesis, physical properties, and applications in medical biotechnology. *J. Nanoparticles.* **2013,** *2013*, e672059, https://doi.org/10.1155/2013/672059.
13. Li, S.; Zhao, Y.; Jiang, Y.; Zhang, Y. Preparation and properties of noble metal core/shell nanostructures prepared by excimer laser ablation in liquid solutions. *J. Laser Appl.* **2014,** *26*, 022001, https://doi.org/10.2351/1.4858315.
14. Tehrani, F.S.; Rasouli, E.; Aliannezhadi, M. Novel photoluminescent In_2O_3/a-SiC core/shell nanostructure synthesized by HW-assisted PECVD method. *Eur. Phys. J. Plus.* **2021**, *136*, 1-14, https://doi.org/10.1140/epjp/s13360-021-01297-z.
15. Barrera, G.; Coisson, M.; Celegato, F.; Olivetti, E.S.; Martino, L.; Miletto, I.; Tiberto, P. Magnetic and thermal characterization of core-shell Fe-Oxide@SiO_2 nanoparticles for hyperthermia applications. *IEEE J. Electromagn. RF Microw. Med. Biol.* **2018,** *2*, 257-261, https://doi.org/10.1109/JERM.2018.2869197.
16. Chatterjee, K.; Sarkar, S.; Rao, K.J.; Paria, S. Core/shell nanoparticles in biomedical applications. *Adv. Colloid Interface Sci.* **2014**, *209*, 8-39, https://doi.org/10.1016/j.cis.2013.12.008.
17. Gawande, M. G.; Goswami, A. G.; Asefa, T.; Guo, H.; Biradar, A.V.; Peng, D.-L.; Zboril, R.; Varma, R.S. Core–shell nanoparticles: synthesis and applications in catalysis and electrocatalysis. *Chem. Soc. Rev.* **2015**, *44*, 7540-7590, https://doi.org/10.1039/C5CS00343A.
18. Bedoya-Hincapie, C.M.; Restrepo-Parra, E.; Lopez-Carreno, L.D. Applications of magnetic and multiferroic core/shell nanostructures and their physical properties. *Dyna.* **2018**, *85*, 29-35, http://www.scielo.org.co/pdf/dyna/v85n207/0012-7353-dyna-85-207-29.
19. Wei, D.-H.; Lin, T.-K; Liang, Y.-C.; Chang, H.-W. Formation and Application of Core–Shell of FePt-Au Magnetic–PlasmonicNanoparticles. *Front. Chem.* **2021,** *9*, 181, https://doi.org/10.3389/fchem.2021.653718.
20. Chaudhuri, R.G.; Paria, S. Core/shell nanoparticles: classes, properties, synthesis mechanisms, characterization, and applications. *Chem. Rev.* **2012**, *112*, 2373-2433, https://doi.org/10.1021/cr100449n.
21. Rawat, D.; Singh, R.R. Avant-grade magneto/fluorescent nanostructures for biomedical applications: Organized and comprehensive optical and magnetic evaluation. *Nano-Struct. Nano-Objects.* **2021**, *26*, 100714, https://doi.org/10.1016/j.nanoso.2021.100714.
22. Reiss, P.; Protiere, M.; Li, L. Core/shell semiconductor nanocrystals. *Small.* **2009**, *5*, 154-168, https://doi.org/10.1002/smll.200800841.
23. Neupane, D.; Ghimire, M. G.; Adhikari, H. A.; Lisfi, A. L.; Mishra, S. M. Synthesis and magnetic study of magnetically hard-soft $SrFe_{12-y}Al_yO_{19-x}$ Wt.% $Ni_{0.5}Zn_{0.5}Fe_2O_4$ nanocomposites. *AIP Adv.* **2017,** *7*, 055602, https://doi.org/10.1063/1.4978398.
24. Dahal, J.N.; Neupane, D.; Mishra, S. Exchange-coupling behavior in $SrFe_{12}O_{19}/La_{0.7}Sr_{0.3}MnO_3$ nanocomposites. *Ceramics.* **2019,** *2*, 100-111, https://doi.org/10.3390/ceramics2010010.